JOURNAL OF Materials CHEMISTRY

Study on the structure and electrochemical properties of melt-spun $Zr_{0.9}Ti_{0.1}(Ni,Co,Mn,V)_{2.1}$ alloys†

Wen Mingfen,*[a] Song Chongli,[a] Chen Lian[b] and Zhai Yuchun[c]

[a]*Institute of Nuclear Energy Technology, Tsinghua University, Beijing 102201, China. E-mail: wmfen@yeah.net*
[b]*Institute of Metal Research, The Chinese Academy of Sciences, Shenyang 110015, China*
[c]*Department of Material and Metallurgy, Northeastern University, Shenyang 110006, China*

Received 13th November 2001, Accepted 16th April 2002
First published as an Advance Article on the web 7th June 2002

The structure and electrochemical properties of $Zr_{0.9}Ti_{0.1}(Ni,Co,Mn,V)_{2.1}$ alloys prepared by both the melt-spinning method and conventional induction melting are investigated. XRD studies show that $Zr_{0.9}Ti_{0.1}(Ni,Co,Mn,V)_{2.1}$ alloys at as-cast, melt-spinning and annealing are all face center cubic structures with a Laves C15 phase and the higher the melt-spinning rate, the greater the amorphous content. The electrochemical measurements show that melt-spun alloys have better active behavior and low discharge capacity (<270 mAh g^{-1}). However, after annealing, the alloys are only activated completely after 30 cycles and the capacities (about 340 mAh g^{-1}) are higher than those of as-cast and just melt-spun alloys; the annealed alloys have a better cycle stability than as-cast alloys, and the higher the melt-spinning rate, the more stable the alloy becomes.

1 Introduction

In recent years, the Ni-Metal hydride (Ni–MH) battery has gradually and steadily replaced the Ni–Cd battery and holds a large share in the secondary battery market. However, its rivals such as the Li-ion secondary battery are challenging the status of the Ni–MH battery. Future prospects of the Ni–MH battery depend on the development of advanced storage alloys with higher capacity and better performance than the commercially used AB_5 alloys.

Zr-based AB_2 type alloys, with a larger hydrogen storage capacity and longer cycle life than the conventional AB_5 alloys and reasonable durability in the electrolyte, are promising candidates as the negative electrode material in the Ni–MH battery.

Many research efforts have been made to improve the activation and kinetic properties of these Zr-based AB_2 type alloys such as the addition of rare earth metals[1] and some pretreatment for instance hot alkaline,[2,3] hot charging treatment[4,5] and a fluorination treatment.[6] In this paper, a melt-spun method was investigated which could improve Zr-based AB_2 alloys cycle stability, we made a more detailed study on the properties of as-cast and melt-spun alloys, and analysed the relationship between microstructure and electrochemical characteristics.

2 Experimental details

An alloy sample of $Zr_{0.9}Ti_{0.1}(Ni,Co,Mn,V)_{2.1}$ was prepared in a vacuum induction furnace under a protective argon atmosphere. In air, the as-cast alloy pieces, called ZAB_2, were mechanically ground; one part was ground to 200 mesh alloy powders, the other part was rapidly solidified into ribbons by the 5T Advanced Melt Spinner (Marko Materials, Inc.). When the rate of the water-cooled molybdenum wheel was controlled (25 m s^{-1}, 40 m s^{-1}), different melt-spun rate alloys were obtained. Some were ground to 200 mesh powder, called qAB_2-25 and qAB_2-40 (for rates of 25 m s^{-1} and 40 m s^{-1}, respectively) and some were annealed at 1173 K for one hour, then ground to 200 mesh powder, called $qHTAB_2$-25 and $qHTAB_2$-40 (25 m s^{-1} and 40 m s^{-1}, respectively).

The electrochemical properties were tested by an Auto charge-discharge instrument made by the Institute of Beijing Nonferrous Metals, China. The process of sample preparation was as follows:

(1) A total weight of 3.0000 g powder of hydrogen storage alloy and nickel powder with the ratio of 1 : 3 was prepared.

(2) The powder was cold-pressed into a 25 mm diameter electrode pellet by a pressure of 30 MPa.

(3) The pellet was sandwiched between two NiOOH/$Ni(OH)_2$ electrodes with excess capacity, and then put into a beaker with 6 M KOH solution at 298 $\pm$ 1 K.

The samples were charged at a current density of 60 mA g^{-1} for 8 h, rested for 5 min, and discharged at the same current density to a cut-off voltage of 1.0 V, and then the maximal discharge capacity was gained.

The cycle life was determined at 300 mA g^{-1} charge–discharge current density.

The crystal structures of the alloys were determined by X-ray diffraction (XRD). XRD was carried on a Rigaku D/max-γ_A diffraction device, Cu Kα radiation and optical filtering with a graphite monochromator. The microstructure of the alloys was observed on a S360 type Scanning Electron Microscope (SEM) from Cambridge Instruments Ltd.

3 Results and discussion

3.1 Microstructure of alloys

Fig. 1 shows that ZAB_2 alloys consist of a large amount of cubic C15 Laves phase, along with a little hexagonal C14

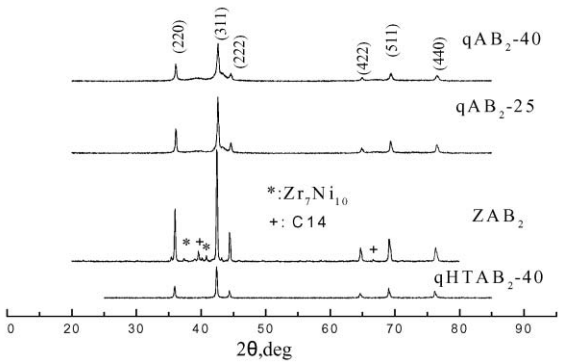

Fig. 1 Diffraction patterns of $Zr_{0.9}Ti_{0.1}(Ni,Co,Mn,V)_{2.1}$ hydrogen storage alloys at different conditions.

†Electronic supplementary information (ESI) available: data used to plot Fig. 4. See http://www.rsc.org/suppdata/jm/b1/b110297d/

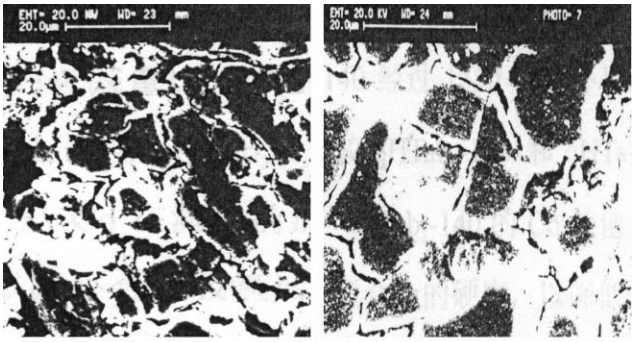

Fig. 2 Surface morphology of $qHTAB_2$-25 and $qHTAB_2$-40 alloys after 1350 cycles.

phase, and non-Laves phase Zr_7Ni_{10}. In the qAB_2-25 and qAB_2-40 alloys the (311) main peak becomes broad, which indicates an amorphous appearance.[7] With increasing melt-spun rate, the intensity of all peaks is reduced. After annealing, the amorphous phase changed into crystals and in $qHTAB_2$-40 only the Laves C15 phase existed.

3.2 SEM photography

Fig. 2 shows the surface morphology of different alloys, obtained by SEM. In Fig. 2, it can be seen that a large number of micro-cracks appear in the alloys after 1350 cycles, especially in $qHTAB_2$-25. The micro-cracks induce solution of elements such as Zr, Ti, which are hydrogen absorbing elements, and Mn, V and Ni, which are beneficial for the kinetic behavior of the alloys. The greater the number of cracks, and the less absorbing hydrogen, the quicker the discharge capacity of the alloy electrode decreases.

3.3 Electrochemical tests

Fig. 3 shows that the active behaviors of the qAB_2-25 and qAB_2-40 alloys, which only need 6–8 cycles to activate completely, are better than that of the $qHTAB_2$-25 alloy, which takes about 30 cycles. The enthalpy of quenching alloys with some amorphous phase is less than 20 KJ mol^{-1}, which indicates that the metal–hydride decomposes easily, but for annealed alloy the enthalpy is more than 30 KJ mol^{-1}, which shows that the bond between the metal and hydrogen is strong and, therefore, desorbing hydrogen is difficult.[7]

From Fig. 3, it can also be seen that the discharge capacities

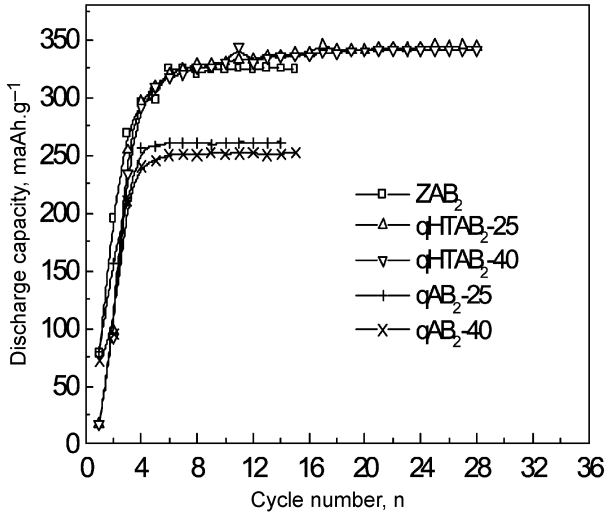

Fig. 3 Discharge capacities of $Zr_{0.9}Ti_{0.1}(Ni,Co,Mn,V)_{2.1}$ hydrogen storage alloys at different conditions as a function of cycle number.

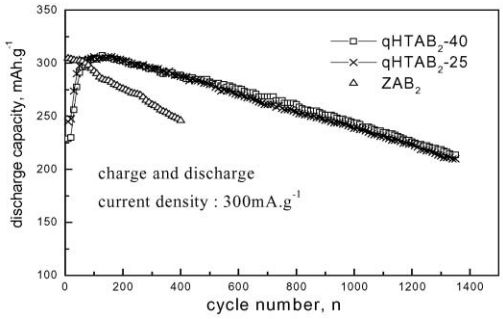

Fig. 4 The cycle stability of $Zr_{0.9}Ti_{0.1}(Ni,Co,Mn,V)_{2.1}$ alloys at different conditions.

of the qAB_2-25 and qAB_2-40 alloys are lower than that of the $qHTAB_2$-25 alloy. In an amorphous alloy, the atoms are disordered and this structure has only a few holes for hydrogen atoms, which means it absorbs little hydrogen, and the discharge capacity is low. The more rapid the cooling rate is, the greater the amorphous content of the alloy, and the lower the discharge capacity. After annealing, the discharge capacity of the $qHTAB_2$-25 alloy is higher than those of the qAB_2-25, qAB_2-40 and ZAB_2 alloys. In annealed alloys, some nano-grains exist, which are beneficial in absorbing–desorbing hydrogen.[8]

Fig. 4 shows the cycle stability of the $qHTAB_2$-25, $qHTAB_2$-40, and ZAB_2 alloy electrodes. It is clear that at a charge–discharge current density of 300 mA g^{-1}, the ZAB_2 alloy is easily activated, while the $qHTAB_2$-25 and $qHTAB_2$-40 alloys need about 100 cycles to be activated completely. The cycle stability of the $qHTAB_2$-25 and $qHTAB_2$-40 alloys is better than that of the ZAB_2 alloy. After 300 cycles, the discharge capacities of the $qHTAB_2$-25 and $qHTAB_2$-40 alloys are about 96% of their maximum capacities, while for the ZAB_2 alloy, it is only 86%. Even after 1350 cycles, the capacity of $qHTAB_2$-40 is still about 70% of the maximum capacity. For annealed alloy, nano-grains existed and the easily oxidized Zr and Mn elements were distributed equally in the alloy, which decreases the rate of oxidation and corrosive rate of the alloy.

3.4 Cycle life model

During cycle life test, the main reasons for the capacity decreasing are oxidization and corrosion. In order to obtain a functional relation between capacity and cycle number some postulates are made as follows:

(1) The particle is powdered at the charge–discharge initial period.

(2) The particle is oxidized at the end of each charge–discharge cycle, and every oxidization depth is the same.

The formula of discharge capacity and cycle number is reduced as follows:

$$M_0 = \frac{4}{3}\rho\pi r_0^3 \tag{1}$$

$$M_1 = \frac{4}{3}\rho\pi r_1^3 = \frac{4}{3}\rho\pi(r_0 - \Delta a)^3 \tag{2}$$

$$M_{N-1} = \frac{4}{3}\rho\pi r_{N-1}^3 = \frac{4}{3}\rho\pi[r_0 - (N-1)\Delta a]^3 \tag{3}$$

$$M_N = \frac{4}{3}\rho\pi r_N^3 = \frac{4}{3}\rho\pi(r_0 - N\Delta a)^3 \tag{4}$$

$$\frac{dM}{dN} = -4\rho\pi\Delta a(r_0 - N\Delta a)^2 \tag{5}$$

$$\frac{dC}{dN} = C_0\frac{dM}{dN} = -4C_0\rho\pi\Delta a(r_0 - N\Delta a)^2 \tag{6}$$

Table 1 The parameters of different alloy electrodes

Alloy	C/mAh g^{-1}	ΔC/mAh g^{-1}	N_{max}
ZAB_2	304.5	0.15	6090
$qHTAB_2$-25	306.25	0.077	11932
$qHTAB_2$-40	305	0.073	12534

Then calculus

$$C = K_0 - 4C_0\rho\pi\Delta a N((r_0 - N\Delta a)^2 - \frac{1}{3}N^2\Delta a^2) \quad (7)$$

where r_0 is particle radius, Δa is the depth of oxidation and corrosion, M is the mass of a solid particle of alloy, ρ is the particle density, C_0 is the maximum discharge capacity, K_0 is constant and N is cycle number.

When

$$r_0 \gg N\Delta a \quad (8)$$

C is linear with N, therefore, from eqn. (6) and (8) it can be seen that:

$$-\frac{4}{3}\Delta C\rho\pi r_0^3 = -4C_0\rho\pi\Delta a r_0^2 \quad (9)$$

$$\Delta a = \frac{r_0}{3C_0}\cdot\Delta C \quad (10)$$

For limited cycle number, the maximum discharge capacity C_0 and ΔC are known. According to formulae (8) and (10), the maximum cycle number N_{max} (*i.e.*, the maximum number of cycles before the relationship between discharge capacity and cycle number ceases to be linear) can be calculated, the results are shown in Table 1.

From Table 1, it can be seen that the maximum cycle number N_{max} is very large, so it can be considered that the discharge capacity is linear with cycle number in this experiment. In order to test the linear relation, the data given in Fig. 4 were linearly regressed as follows: $y = A + Bx$, where y is capacity, x is cycle number, A and B are constant. The results are shown in Table 2.

Table 2 shows that the capacity of all the electrodes is linear with cycle number, in which the correlation coefficient (R) is up to 99%. Therefore, for a limited cycle number, the decrease in capacity ΔC of each cycle can be calculated and the maximum capacity is known. As the capacity is linear with cycle number, the cycle life of alloy electrode can be forecasted. We can economize by using this model to forecast the electrode cycle life instead of taking a long time to test the cycle life.

Table 2 The linear parameters of different alloy electrodes

Alloy	A/mAh g^{-1}	B/mAh g^{-1}	R
ZAB_2-1	308.02	−0.156	−0.997
$qHTAB_2$-25	318.61	−0.0801	−0.999
$qHTAB_2$-40	318.53	−0.0754	−0.997

4 Conclusion

The annealed alloy electrode has a bigger discharge capacity than that of the as-cast electrode, and has a longer cycle life. The cycle life can be calculated by our model, which allows us to greatly economize test time. The alloy can be used in powerful batteries, especially in electrical vehicles.

References

1 C. Iwakura, I. Kiwn and N. Matsul, *Electrochim. Acta*, 1995, **40**, 561.
2 D. Y. Yan, G. Sandroch and S. Suda, *J. Alloys Compd.*, 1994, **216**, 237.
3 J. H. Jung, H. H. Lee and D. M. Kim, *J. Alloys Compd.*, 1997, **253–254**, 652.
4 B. H. Liu, J. H. Jung and H. H. Lee, *J. Alloys Compd.*, 1996, **245**, 132.
5 J. H. Jung and K. Y. Lee, *J. Alloys Compd.*, 1995, **226**, 166.
6 R. Mishima, H. Miyamura and T. Sakai, *J. Alloys Compd.*, 1993, **192**, 176.
7 L. Chen, F. Wu and M. Tong, *J. Alloys Compd.*, 1999, **293–295**, 508.
8 Z. Andreas, C. Daniel and N. Christof, *J. Alloys Compd.*, 1998, **266**, 321.